Available online at www.sciencedirect.com
ScienceDirect
Journal of Solid State Chemistry 181 (2008) 150–157
JOURNAL OF SOLID STATE CHEMISTRY
www.elsevier.com/locate/jssc

Formation of Si–C–N ceramics from melamine–carbosilazane single source precursors

Mazin Shatnawi, Wafaa Al-Mansi, Isam Arafa*

Faculty of Science, Department of Applied Chemistry, Jordan University of Science and Technology, P.O. Box 3030, Irbid 22110, Jordan

Received 19 July 2007; received in revised form 23 October 2007; accepted 11 November 2007
Available online 17 November 2007

Abstract

A series of melamine–carbosilazane pre-ceramic macromolecules (Mel–CSZs) were prepared by the condensation of melamine with different organochlorosilanes (R_xSiCl_{4-x} where R is CH_3/C_6H_5 and x is 1, 2 or 3) using pyridine as a solvent under nitrogen atmosphere. These melamine-based carbosilazane macromolecules (Mel–CSZs) were characterized by infrared spectroscopy (FT-IR), mass spectrometry (MS), thermogravimetric analysis (TGA) and differential scanning calorimetry (DSC). The backbone of the resulting Mel–CSZs consists of melamine and carbosilazane building blocks. Pyrolysis of these Mel–CSZs at 600 °C under nitrogen and vacuum afforded the corresponding silicon-based nonoxide carbonitride ceramics (Si–C–N). The microstructure and textural morphology of the resulting fine ceramic materials were examined using FT-IR, powder X-ray diffraction (XRD), and scanning electron microscopy (SEM).

Keywords: Pre-ceramic; Nonoxide ceramic; Melamine composite; Si–C–N; Organosilicon

1. Introduction

Binary, ternary and quaternary main group nitrides have been the subject of intensive research for many years [1–9]. In particular, nitrides of group 13 (B, Al, Ga, In) and 14 (C, Si, Ge Sn) are reported to exhibit unique optical, thermomechanical, structural stability and opto-electronic properties [4,10–13]. Recent years have witnessed a growing interest in amorphous and crystalline carbon nitrides (C_3N_4) [11–17]. Novel techniques such as arc discharge, laser ablation, sol–gel processing, chemical vapor deposition (CVD), high-energy ball milling, sol-vothermal, electrodeposition and pyrolysis have been developed for the synthesis of interesting phases of C_3N_4 such as nanotubes, nanospheres, cubic, two-dimensional (2-D) graphitic, α- and β- forms [11–17]. Since Teter and Hemlay [18] suggested melamine (2,4,6-triamino-1,3, 5-triazine) as a potential precursor for obtaining C_3N_4, several research groups have exploited members of the 1,3,5-triazine ring system such as melamine (I), cyanuric acid (II) and chlorocyanuric acid (III) as precursors for polymeric carbon nitride-based materials [11,13,15,16,19]. Thermal degradation of melamine under high pressure and temperature conditions occurs through the formation of melam and melem intermediates and finally affords 2-D g-C_3N_4 [11,15].

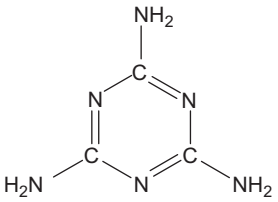

I

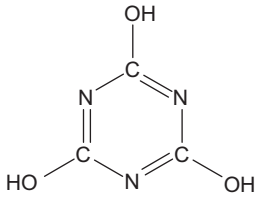

II

*Corresponding author. Fax: +962 2 7095014.
E-mail address: isamaraf@just.edu.jo (I. Arafa).

0022-4596/$ - see front matter © 2007 Elsevier Inc. All rights reserved.
doi:10.1016/j.jssc.2007.11.009

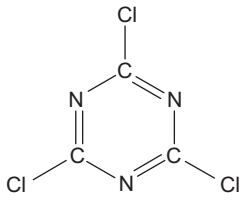

III

On the other hand, silicon-based binary, ternary and quaternary nitride ceramics (Si–N, C–Si–N, O–Si–N, Si–B–C–N) largely rely on silicon-containing precursors for protective coating, fibers, sensors, bio-ceramics and other electronic devices [1–5,7–9]. In fact, organosilicon polymers possessing Si–N, C–Si–N and Si–B–C–N bonds in their backbones such as polysilazane, polycarbosilazane, polyborosilazane and polyborocarbosilazane are often employed as single-source precursors for obtaining the desired silicon-based nitride ceramics [1–3,5,7,9].

In this paper, we report the preparation of different melamine–carbosilazane macromolecules (Mel–CSZ) from the reaction of melamine (I) with different organochlorosilane reagents (R_xSiCl_{4-x}, where R is CH_3, C_6H_5 and x is 1,2,3) in pyridine under nitrogen atmosphere. To our best knowledge, this is the first report on 1,3,5-triazine-based organosilicon oligomers. The resulting oligomers are characterized by infrared (FT-IR), mass spectrometry (MS), thermogravimetric analysis (TGA) and differential scanning calorimetry (DSC). Thermolysis/pyrolysis of the obtained Mel–CSZs at relatively low temperatures (>600 °C) under nitrogen and vacuum afforded Si–C–N ceramics with different compositions, nanostructures and morphologies. The microstructure and morphology of the obtained Si–C–N ceramics are examined by FT-IR, X-ray diffraction (XRD) and scanning electron microscopy (SEM) techniques.

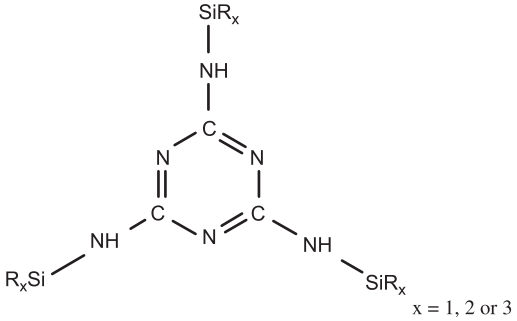

2. Experimental

2.1. Materials and methods

All chemicals and solvents were reagent grade and used as received without further purification. Pyridine (BDH) was dried over molecular sieves. Melamine, trichloromethylsilane, chlorotrimethylsilane and trichlorophenylsilane were purchased from Aldrich. Dichlorodimethylsilane, dichlorodiphenylsilane and chlorotriphenylsilane were obtained from Acros Organics.

FT-IR spectra were recorded on a Nicolet Impact 410 FT-IR spectrophotometer as KBr pellets. MS was performed on a VGA-7070 (EI, 70 eV). TGA and DSC were carried out under nitrogen atmosphere (temperature range = 20–500 °C, heating rate = 10 °C/min) on Shimadzu TGA-50 and DSC-50 systems equipped with a computerized data station TA-5 WS/PC, respectively. Powder XRD was obtained on a Philips, PW 1729 X-ray spectrometer using Cu ($K\alpha_1$, $\lambda = 1.5404$ Å) generated at 35 kV (40 mA) and $2\theta = 5$–$100°$ with 0.04° increments. The textural morphology of the pyrolized materials investigated on SEM-FEI Philips microscope. The samples were sputter coated with gold (1200, 20 kV, Polaron E6100).

2.2. Synthesis of melamine–carbosilazane macromolecules (Mel–CSZs)

All these macromolecules were prepared by refluxing melamine with the desired molar ratio of alkyl- and aryl-chlorosilane reagents in pyridine under nitrogen atmosphere. A summary of the preparation conditions and results is presented in Table 1. In a typical procedure, melamine (12.60 g, 100 mmol) was suspended in pyridine (~150 ml) in a 250 ml three-neck round bottom flask equipped with a condenser, a dropping funnel and a magnetic stirring bar under nitrogen atmosphere. Diphenyldichlorosilane (37.98 g, 150 mmol) in the dropping funnel was slowly added with continuous stirring. The reaction mixture was refluxed for 5–6 h, during which pyridinium–hydrochloride salt precipitates. The reaction mixture was cooled to room temperature and left overnight under nitrogen, after which the pyridinium–hydrochloride salt was filtered off. The pyridine was removed at reduced pressure, leaving behind a viscous waxy product. The crude product was washed with chloroform 3–4 times and finally dried under vacuum to a constant weight.

2.3. Conversion of Mel–CSZs into Si–C–N ceramics

The obtained Mel–CSZs were cured by heating at 120 °C under nitrogen for 8 h and left under nitrogen for about 4–5 days at 95 °C. Pyrolysis was carried out at 600 °C under nitrogen, vacuum and air. In all cases, the temperature was raised to 300 °C (heating rate = 20 °C/min), maintained for 30–60 min and then increased further to 600 °C for 6 h. The microstructure and morphology of the resulting ceramic products were examined by FT-IR, powder XRD and SEM.

3. Results and discussion

3.1. Synthesis and characterization

Condensation reactions of melamine with different alkyl- and aryl-chlorosilanes (R_xSiCl_{4-x}, $R = CH_3$, C_6H_5; $x = 1$,

Table 1
Physical properties and elemental analysis of the prepared Mel–CSZs

Mel–CSZs	Melamine mmol (g)	Organosilane mmol (g)	Reflux time (h)	% Yield	Color/state	M. wt[a] (*n*)
Mel–SiPh	100 (12.60)	$PhSiCl_3$ 103 (21.79)	10–12	56	White powder	682 (3)
Mel–$SiPh_2$	100 (12.60)	Ph_2SiCl_2 150 (37.98)	5–6	36	Greenish waxy solid	418 (2)
Mel–$SiPh_3$	23.8 (3.00)	Ph_3SiCl 71 (21.04)	4–5	84	Off white powder	890 (1)
Mel–SiMe	100 (12.60)	$MeSiCl_3$ 71 (15.45)	10–12	38	Grey waxy solid	551 (3)
Mel–$SiMe_2$	100 (12.60)	Me_2SiCl_2 150 (19.36)	5–6	32	Creamy waxy solid	1462 (5)
Mel–$SiMe_3$	79 (10.00)	Me_3SiCl 238 (25.84)	4–5	16	Off-white waxy solid	332 (1)

[a]The molecular weight was determined cryoscopically in DMF. *n* is the degree of polymerization.

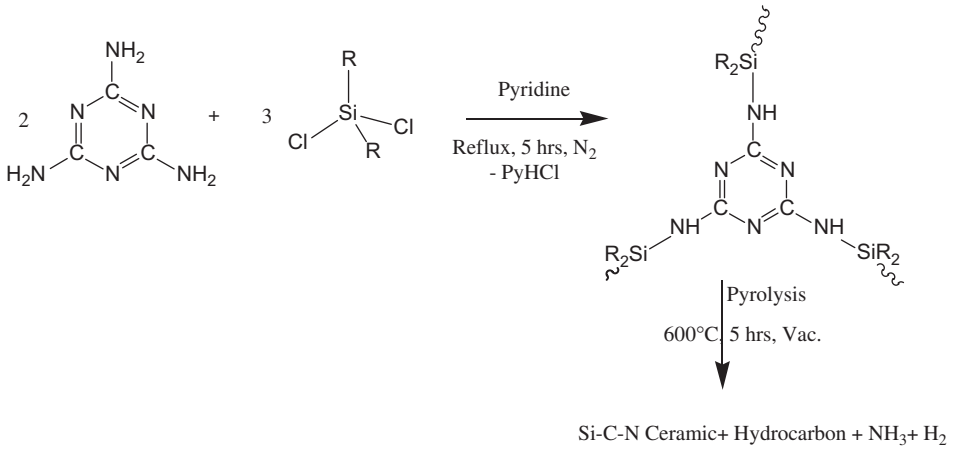

Scheme 1.

2, 3) in refluxing pyridine under nitrogen atmosphere resulted in the formation of the desired Mel–CSZ, Scheme 1. Pyridine serves as both a solvent and a weak base. The color, state, molecular weights and degree of polymerization of the resulting materials are summarized in Table 1. Qualitative end-group analysis using methanolic solutions of $AgNO_3$ showed the presence of chloride in all cases except in Mel–$SiPh_3$ macromolecules. This observation is in agreement with the low molecular weight and low degree of polymerization ($n = 2$–5) data. However, these low molecular weight Mel–CSZs are further condensed by annealing (curing) for several days before pyrolysis experiments. All these Mel–CSZs form a colloidal solution in DMSO, DMF and to some extent in acetone. These macromolecules were characterized by FT-IR spectroscopy, MS, TGA and DSC techniques.

Pyrolysis of polymeric precursors under appropriate conditions has often been employed for obtaining non-oxide ceramics [1,11,15,16,19]. Successful utilization of this pyrolysis method mainly relies on the synthesis of suitable pre-ceramics with defined structures and properties, i.e. latent reactivity which allows for cross-linking reactions during thermolysis thereby preventing excessive weight loss. It is important to point out that the mechanical, textural and functional properties of the final ceramic material strongly depend not only on the pyrolysis procedure but also on the composition and microstructure of the precursor. Furthermore, this method allows the preparation of nonoxide ceramics in different ceramic forms and shapes (fibers, thin films and membranes) at relatively low processing temperatures.

The prepared Mel–CSZ macromolecules were cured by heating under nitrogen at 120 °C (8 h) and then left in nitrogen atmosphere at 95 °C for 4–5 days. The cured Mel–CSZ macromolecules were re-examined by FT-IR, TGA and DSC. Comparison between the thermal data for the cured and the uncured samples indicates that further condensation processes took place. However, the FT-IR spectra of cured and uncured Mel–CSZs products indicated that they are practically similar. The cured Mel–CSZs were subjected to pyrolysis at 600 °C in air, nitrogen and vacuum. Pyrolysis in open air afforded a white SiO_2 powder that dissolves in excess aqueous HF as shown below. The identity of the product was confirmed by FT-IR spectroscopy. However, the inert atmosphere and vacuum pyrolysis resulted in the formation of

$$SiO_2 + \text{excess HF} \rightarrow H_2SiF_{6(aq)} + H_2O,$$

$$Si{-}C{-}N + \text{excess HF} \rightarrow \text{no reaction.}$$

hard dark grey-black solid materials. The obtained ceramics were washed with HF to remove any silicon

Table 2
Nonoxide ceramic yield obtained from the pyrolysis of Mel–CSZs at 600 °C under nitrogen and vacuum

Mel–CSZs	Ceramic yield (%)	
	Nitrogen	Vacuum
Mel–SiMe	21	34
Mel–$SiMe_2$	11	3
Mel–$SiMe_3$	41	1
Mel–SiPh	20	14
Mel–$SiPh_2$	19	16
Mel–$SiPh_3$	15	38

oxide formed. The ceramic yields for the pyrolysis under inert atmosphere and vacuum are summarized in Table 2. The wide difference in the ceramic yield may be attributed to sublimation of intermediate species that suggests a different pyrolytic mechanism. In fact, the escaped gases were examined chemically and showed that they are ammonia/organic amines [15,16]. It should be noted that the FT-IR of the pyrolyzed products display similar spectra (see FT-IR section). The microstructure and morphology of the resulting fine ceramic materials were examined using FT-IR, powder-XRD and SEM.

At this stage, three interesting observations are worth noting. First, no observable changes (visually and by HF test) were noted when the obtained nonoxide ceramics were further subjected to flame pyrolysis in open air (exposure to direct flame). This clearly indicates that the obtained non-oxide ceramics are stable towards thermo-oxidative conditions. Second, when the Mel–CSZs are solvent coated onto microscopic slides or metal surfaces and then pyrolyzed under inert atmosphere, the resulting nonoxide ceramic products adhere strongly to the surfaces. Third, pyrolysis of phenyl-containing Mel–CSZs yielded smooth shiny surfaces (see SEM section).

3.2. FT-IR spectroscopy

The spectra for the obtained Mel–CSZ macromolecules were recorded in the region of 400–4000 cm^{-1} as KBr pellets. The characteristic absorption infrared bands are presented in Table 3. All these macromolecules exhibit a band around 3300 cm^{-1} assigned to the N–H stretching mode. The absence of asymmetric stretching frequency for N–H band and the presence of new bands due to ν_{Si-N} indicate the formation of Si–N bonds in Mel–CSZs. Of a particular importance is the $\delta_{Si-}CH_3$ frequency which appears at about 1260 cm^{-1} in the methyl-containing Mel–CSZs and δ_{Si-Ph} at about 1430 and 1100 cm^{-1} in phenyl-containing Mel–CSZ products [9]. Furthermore, the IR bands within the range 1600–1400 cm^{-1} are diagonistic for triazine rings [13]. The multiple bands that appear in the 800–600 cm^{-1} region due to δ_{Si-C} and δ_{Si-N} support the above conclusion.

The characteristic FT-IR absorption bands for the obtained non-oxide ceramic materials are summarized in Table 4. Since there is a possibility for the formation of different silicon carbide (Si–C), silicon–nitride, graphitic carbonitride (g–C–N), and graphite–carbon phase (g–C), the FT-IR spectral data should be taken with caution [11–16]. In fact, the FT-IR spectra should be interpreted in conjunction with XRD and SEM data. The drastic decrease in the intensity of ν_{N-H} ν_{C-H} characteristic peaks indicates that amino and methyl/phenyl groups have undergone thermal degradation, leaving behind silicon carbonitride (Si–C–N) ceramic residues. The presence of broad peaks in the range of 1600–1650 cm^{-1} due to g–C appears clearly in the FT-IR spectra of Mel–$SiPh_3$. FT-IR peaks at 835 and 900–950 cm^{-1} are attributed to the stretching frequencies of Si–N and N–Si–N/O–Si–N. The peaks at 815 and 750 cm^{-1} imply the presence of Si–C bond in the final ceramics. Close inspection of the FT-IR spectrum of the pyrolyzed Mel–$SiMe_2$ shows a number of overlapping peaks in 1300–1000 cm^{-1} range that suggest the presence of more than one ceramic phase.

Table 3
FT-IR spectral data for Mel–CSZ macromolecules recorded as KBr pellets

Mel–CSZ	Wavenumber (cm^{-1})
Mel–SiMe	3330; 2920; 1260; 1115; 1050; 1005; 810; 765; 710; 600
Mel–$SiMe_2$	3370; 2920; 1265; 1115; 1011; 810; 755; 690; 595; 570
Mel–$SiMe_3$	3336; 2920, 2850; 1252; 1160; 1152; 1056; 998; 810; 770; 695; 600; 585
Mel–SiPh	3336; 3036; 1429, 1133; 1070; 1005; 780; 690; 680; 510
Mel-$SiPh_2$	3351; 3061; 1435, 1126; 1050; 995; 750; 760; 700; 545; 500
Mel–$SiPh_3$	3254; 3061, 2997; 1430, 1114; 1080; 1000; 845; 715; 735; 700; 530

Table 4
FT-IR spectral data for pyrolyzed Mel–CSZs under nitrogen and vacuum*

Pyrolysis product	Under N_2 wavenumber (cm^{-1})	Under vacuum wavenumber (cm^{-1})
Mel–SiMe	1281; 1150, 1056; 786	1280; 1114, 1024; 786, 715
Mel–$SiMe_2$	1236; 1180, 1075; 815	1274; 1126, 1056; 805
Mel–$SiMe_3$	1236; 1185, 1115; 810, 735	1249; 1085,1015; 805, 765, 690
Mel–SiPh	1204; 1075; 790	1230; 1140, 1080; 800, 700
Mel–$SiPh_2$	1133; 1049; 786, 700	1210; 1140, 1049; 799, 760,705
Mel–$SiPh_3$	1197; 1081, 1050; 798	1220; 1075, 1030; 798, 700

*Recorded as KBr pellets.

3.3. Mass spectrometry (MS)

The prepared Mel–CSZ macromolecules were examined by mass spectrometry. All fragments with relative intensity >4% and their tentative assignments are given in Table 5.

Table 5
Mass spectrometric data and assignments for the Mel–CSZ macromolecules[a]

Mel–CSZs	m/z (Relative intensity %), assignment
Mel–SiMe	36 (92)[b]; 52 (96) $C_2N_2^+$; 75 (14) $SiMe(NH_2)_2^+$; 79 (99) $HC_3N_3^+$; 149 (6) $HSi(NCN)_3^+$
Mel–$SiMe_2$	52 (71) $C_2N_2^+$; 73 (100) $SiMe_2NH^+$; 147 (24) $C_3N_6H_2^+$; 282 (16) $Mel(SiMe_2)_2SiMe^+$; 356 (18) $Mel(SiMe)_3(SiMeNH_2)^+$; 430 (12) $Mel(SiMe)_3(SiMeNH_2)_2^+$, 505 (13) $HMel_2(SiMe_2)_3(SiCH_2)_2^+$, 579 (4) $Mel_2(SiMe_2)_5SiMe^+$
Mel–$SiMe_3$	43 (72) $SiMe^+$; 52 (60) $C_2N_2^+$; 57 (82) $MeSiCH_2^+$; 69 (53) $MeSiCN^+$; 79 (78) $HC_3N_3^+$; 97 (22) $Me_2CH_2SiCN^+$; 109 (9) $HSi(NCN)_2^+$; 111 (10) $SiMe_3NH_2CN^+$
Mel–SiPh	36 (90)[c]; 52 (97) $C_2N_2^+$; 79 (100) $HC_3N_3^+$; 126 (8) H_3Mel^+; 149 (4) $HSi(NCN)_3^+$
Mel–$SiPh_2$	52 (100) $C_2N_2^+$; 79 (100) $HC_3N_3^+$; 154 (20) $(C_6H_5)_2^+$; 181 (6) $SiC_6H_5C_6H_4^+$; 440 (6) $H_2Mel(SiC_6H_5)_3^+$
Mel–$SiPh_3$	45 (20) $SiNH_3^+$; 77 (29) $C_6H_5^+$; 122 (31) $Si(C_6H_5)NH_3^+$; 199 (100) $Si(C_6H_5)_2NH_3^+$; 277 (44) $Si(C_6H_5)_3NH_3^+$

H_2NCN = cyanamide.
[a]EI, 70 eV.
[b]Mel = $C_3N_3(NH)_3$.
[c]This fragment appears to be due to doubly charged silicon carbonitrides.

In most cases, the presence of a high-intensity mass spectral fragment at m/z of 52 and 79 are assigned to $C_2N_2^+$ (cyanogene) and/or $HC_3N_3^+$ (protonated triazine ring), respectively. This clearly indicates that triazine ring is an integral part of the structure. Furthermore, fragments due to methyl- or phenyl-containing carbosilazane segments are clearly observed as shown in Table 5. These observations are consistent with the fact that the structures of these Mel–CSZs are composed of melamine and carbosilazane segments. Moreover, the low-intensity fragments due to high m/z values clearly demonstrate that Mel–$SiMe_2$ ($m/z = 579$) and Mel–$SiPh_2$ ($m/z = 440$) are macromolecular in nature (dimmers–trimers) (Fig. 1).

3.4. Thermal analysis

The thermal behavior of the prepared Mel–CSZ macromolecules was investigated using TGA and DSC (N_2 atmosphere, heating rate = 10 °C/min, temperature range of 25–500 °C). The thermal events below 100 °C correspond to the removal of solvents entrapped into Mel–CSZ lattices. It is obvious from TGA data in Table 6 and the corresponding thermograms in Fig. 2 that all these materials except Mel–SiPh display two major thermal degradation steps in the temperature range of 150–250 and 250–350 °C with an overall mass loss of 76–96%. Furthermore, the amount of residue in the case of Mel–$SiMe_3$ and Mel–$SiPh_3$ is low (4–7%). A close examination of the data in Table 6 shows that the phenyl-containing Mel–CSZs afforded higher ceramic yields than the corresponding methyl-containing Mel–CSZs.

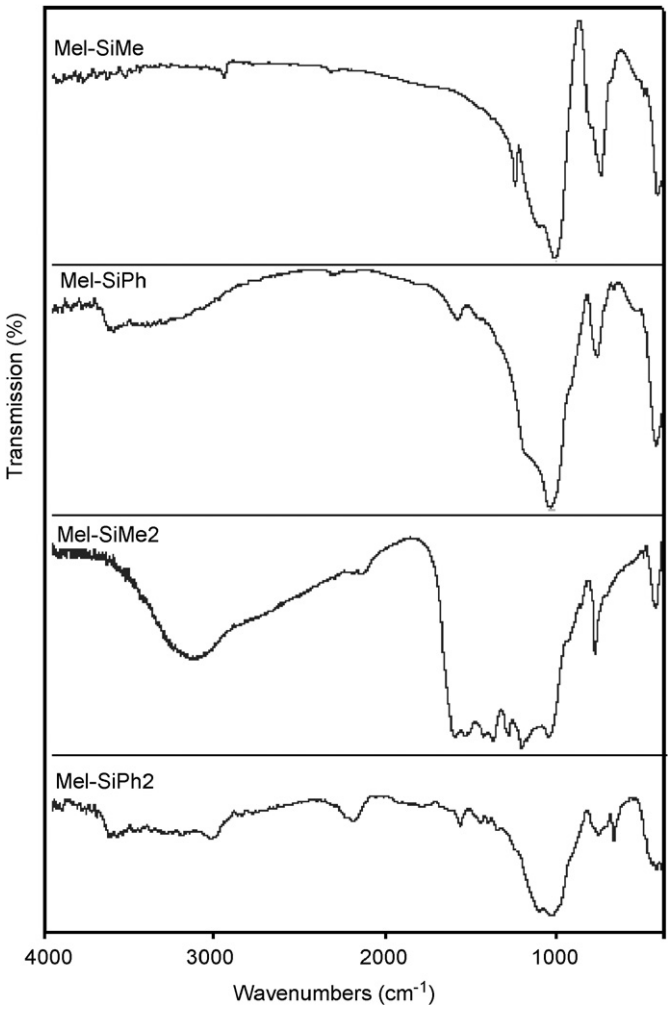

Fig. 1. FT-IR spectra of the ceramic products obtained from the pyrolysis of bifunctional and trifunctional Mel–CSZs.

Table 6
Thermogravimetric analysis (TGA) data for the uncured Mel–CSZ macromolecules[a]

Mel–CSZs	Degradation temperature °C (% Mass loss)			% Mass	
	Step 1	Step 2	Step 3	Volatile[b]	Residue[c]
Mel–SiMe	145 (65)	290 (15)	–	3	17
Mel–$SiMe_2$	117 (30)	305 (40)	427 (15)	7	8
Mel–$SiMe_3$	160 (34)	280 (60)	–	2	4
Mel–SiPh	150 (76)	–	–	[d]	24
Mel–$SiPh_2$	135 (43)	364 (39)	–	3	15
Mel–$SiPh_3$	–	240 (50)	378 (43)	[d]	7

[a]Conditions: N_2 atmosphere, temperature range = 25–500 °C, heating rate = 10 °C/min.
[b]Components lost below 100 °C.
[c]Residue > 500 °C.
[d]Negligible.

Fig. 3 displays the DSC heating curves of the obtained Mel–CSZ macromolecules. In all cases, the observed overlapping endotherms between 100 and 400 °C are

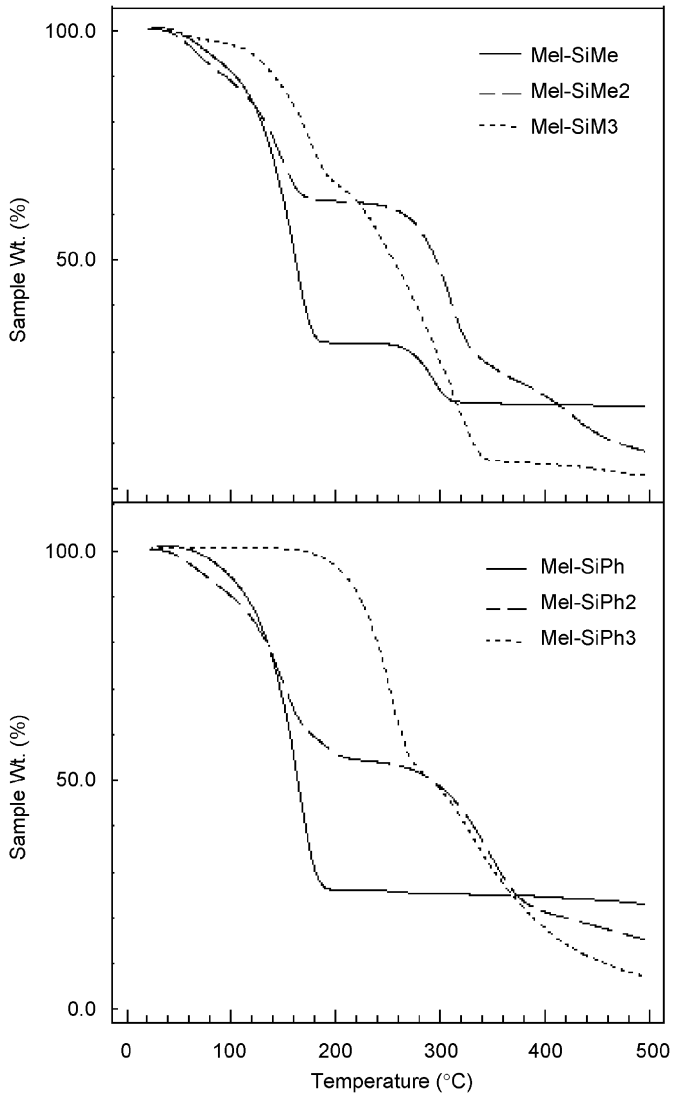

Fig. 2. TGA plots for the prepared Mel–CSZ macromolecules.

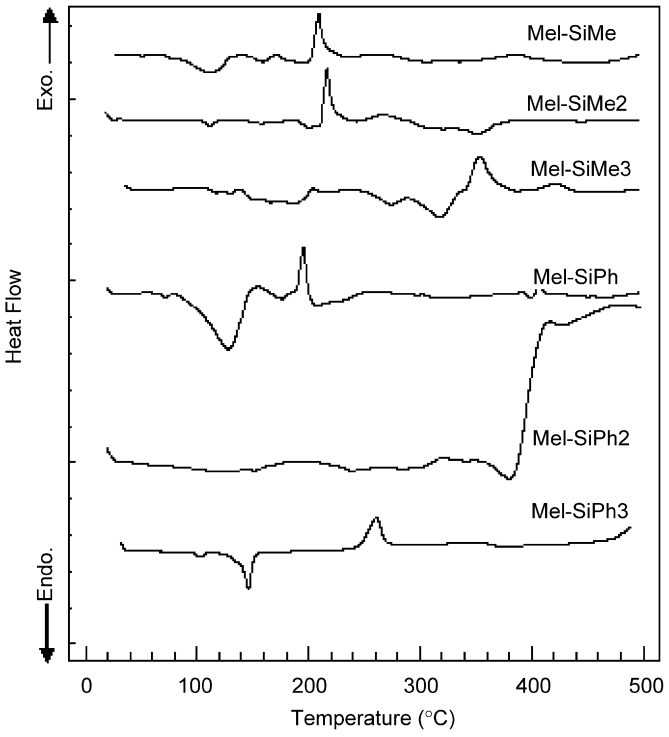

Fig. 3. DCS curves of the prepared Mel–CSZ macromolecules.

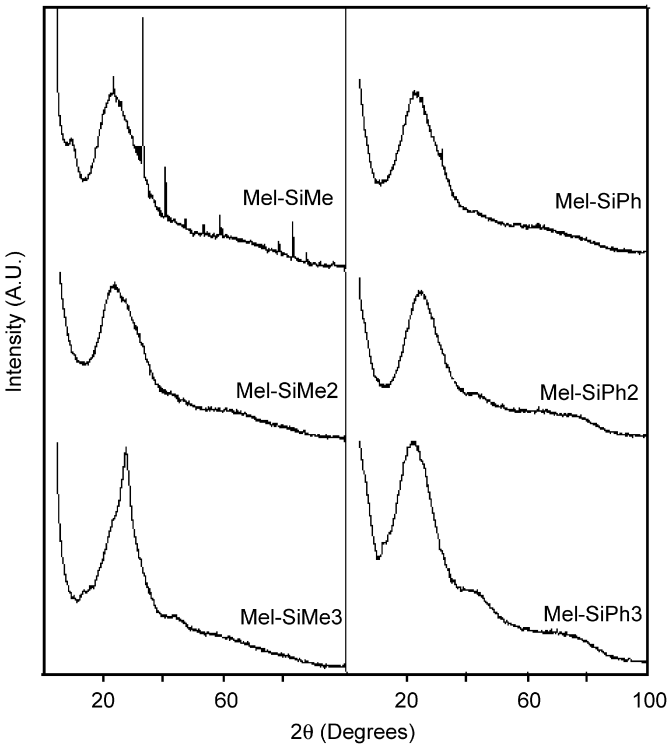

Fig. 4. Powder XRD patterns of the ceramic products obtained from the pyrolysis of the melamine-based carbosilazane macromolecules.

attributed to step-wise thermal decomposition processes. In this context, the reported DSC curve of melamine shows two thermal events due to melting (363 °C), followed by the formation of melem (360–380 °C) that is further converted to g–C_3N_4 materials at ~580 °C [15]. The observed thermal events in Mel–CSZs clearly demonstrate that the melamine building block in Mel–CSZs behaves in a different fashion compared with that of free melamine. Close analysis of the shapes of the DSC traces in the light of the TGA data suggests that their decomposition pathways are very complicated. In other words, each degradation step observed in TGA is composed of multiple thermal DSC events. This observation is obvious in the case of Mel–SiPh, where the TGA curve displays a one-step decomposition at ~166 °C whereas the corresponding DSC thermogram is composed of four endotherms due to the decomposition and relaxation, and one exotherm at ~200 °C due to crystallization of the decomposed products. This observation implies that thermal relaxation and crystallization processes follow the first decomposition step. Interestingly, the first endotherms observed for Mel–SiMe and Mel–SiPh products are much larger than those observed for the Mel–$SiMe_2$ and Mel–$SiPh_2$, and in turn larger than that of the Mel–$SiMe_3$ and Mel–$SiPh_3$

materials. This implies that the lost moiety is present in large proportion in the tri-functional compared to bi-functional and mono-functional systems. This step may be assigned to the loss of amine groups of the melamine segments. In fact, upon heating ammonia/organic amines gases escape, which are consistent with degradation of melamine. Furthermore, the TGA and DSC curves for the prepared Mel–CSZs before and after heat curing are practically similar in shape but different in residues %. This similarity is also confirmed by the FT-IR spectral data (see FT-IR section).

Table 7
Powder XRD data of the pyrolyzed Mel–CSZs under N_2 atmosphere

Mel–CSZs	2θ (degrees)	d (Å)[a]
Mel–SiMe	9.0, 23.2[b], 32.9 (s), 40.4 (s), 58.5, 78.1, 82.6, 87.2	3.83
Mel–$SiMe_2$	23.6[b], 30.0 (sh)	3.77
Mel–$SiMe_3$	23.3(sh) 27.2[b]	3.28
Mel–SiPh	23.5[b], 31.8 (s), 50.2 (s), 63.7 (s)	3.78
Mel–$SiPh_2$	24.9[b], 42.8, 64.4.	3.57
Mel–$SiPh_3$	23.0[b], 43.6	3.86

S = sharp, sh = shoulder.
[a]Calculated from Braggs' Law ($n\,\lambda = 2\,d\sin\theta$).
[b]Broad peaks used to calculate the d-spacings.

3.5. Powder X-ray diffraction (XRD)

Information about the microstructure and allotropic phases of nonoxide ceramics can be conveniently inferred from the powder-XRD diffraction patterns. Fig. 4 displays the XRD profiles obtained for the pyrolyzed Mel–CSZ macromolecules under nitrogen atmosphere. The broad

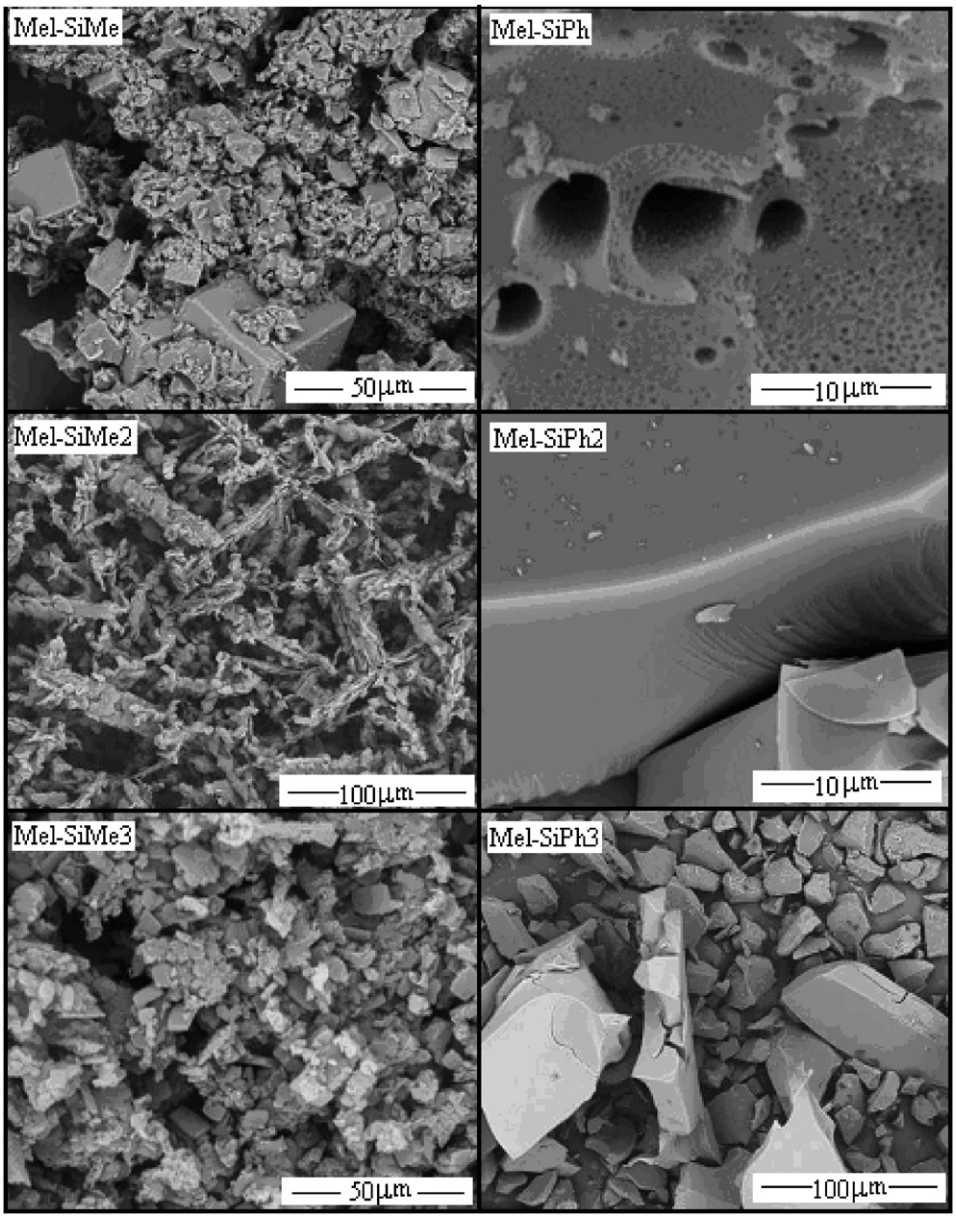

Fig. 5. SEM images of ceramic products obtained from the pyrolysis of the melamine-based carbosilazane macromolecules.

diffraction peaks observed in all XRD profiles indicate that the obtained nonoxide ceramic materials are largely amorphous in nature [2,4]. Close inspection of the broad diffraction patterns of Si–C–N ceramics indicates that the main broad peak is composed of two overlapping diffraction peaks located at a 2θ range of 23.0–27.2°. This observation suggests that the obtained Si–C–N materials may contain two different sub-lattices, that is supported by SEM image analysis (see section on SEM). The position of the most intense broad diffraction peak and the corresponding interspatial distances are listed in Table 7. In these nonoxide ceramics, the *d*-spacing ranges between 3.28 and 3.86 Å. It is interesting to state that g–C_3N_4 materials exhibit a single main diffraction peak due to (002) plane, which corresponds to the *d*-spacing of interlayer distance of 3.2–3.4 Å [11,13,14]. Furthermore, the sharp diffraction features in the Mel–SiMe ceramic clearly show a small crystalline Si–C–N phase co-existing with the amorphous phase. This sharp diffraction pattern is typical for Si–C–N crystalline phase [7,9,20].

On the other hand, the nonoxide ceramics obtained from the phenyl-containing Mel–CSZ exhibit a single broad diffraction peak suggesting that these materials are monophasic amorphous materials. This conclusion is strongly supported by the SEM images of these materials. In fact, crystalline nonoxide ceramics form at much higher temperatures than that adopted in our experiment (600 °C).

3.6. Scanning electron microscopy (SEM)

Fig. 5 displays the SEM images of the pyrolyzed Mel–CSZs under nitrogen. It is clear that the obtained images indicate different surface morphology and structure. This observation is consistent with the fact that the textural morphology of the pyrolyzed products largely relies on the structure and composition of their precursors [5]. In short, the phenyl-containing Mel–CSZs form smooth surfaces compared with those of methyl-based Mel–CSZ precursors. Interesting morphological features are observed in the case of Mel–$SiMe_2$, Mel–SiPh and Mel–$SiPh_2$. In the case of Mel–$SiPh_2$ the surface was smooth and reflecting, suggesting potential application in coating industry. In this respect, it is important to note that when this material is applied to a glass or metal substrate, before being pyrolyzed, it forms a compact strongly adhering thin film. However, Mel–SiPh exhibits smooth surfaces with spongy-like structure of different cylindrical pores with a diameter of 1–10 μm. Potential applications of such materials in gas absorption, gas separation and catalysis are anticipated. Surprisingly, the textural morphology of pyrolyzed Mel–$SiMe_2$ afforded rod-like structures with strongly adhered fine crystallite particles. The formation of this biphasic material is supported by the FT-IR spectroscopy and powder-XRD. However, Mel–SiMe, Mel–$SiMe_3$ and Mel–$SiPh_3$ gave particles with irregular shapes and sizes. It is interesting to note that a monolith of Mel–$SiPh_3$ underwent cracking during SEM experiments leading to small high reflecting smooth particles with sharp edges.

4. Conclusion

Mel–CSZ prepared by one-pot condensation reaction of melamine with different organochlorosilanes (R_xSiCl_{4-x} ($R = CH_3$, C_6H_5, and $x = 1, 2, 3$) offer a convenient route for the formation of valuable precursors for Si–C–N nonoxide ceramics. The XRD and SEM studies indicate that pyrolyzed Mel–CSZs ceramics are amorphous in nature with obvious heterogeneous microstructure. The composition and structure of these versatile macromolecules permit one to prepare nonoxide ceramics with interesting microstructure, surface and textural properties. In particular, the surface properties of the nonoxide ceramic derived from Mel–$SiPh_2$ and Mel–SiPh are currently under further investigation for their potential technological applications in protective coating and in the preparation of metalloceramics.

Acknowledgment

Financial support from the Deanship of Research at the Jordan University of Science and Technology is gratefully acknowledged.

References

[1] M. Birot, J. Pillot, J. Dunogues, Chem. Rev. 95 (1995) 1443–1477.
[2] H. Wang, S. Zheng, X. Li, D. Kim, Microporous Mesoporous Mater. 80 (2005) 357–362.
[3] S. Bernard, M. Weinmann, P. Gerstel, P. Miele, F. Aldinger, J. Mater. Chem. 15 (2005) 289–299.
[4] I. Sung, C. Mitchell, D. Kim, P. Kenis, Adv. Funct. Mater. 15 (2005) 1336–1342.
[5] T. Wideman, P. Fazen, K. Su, E. Remsen, G. Zank, L. Sneddon, Appl. Organometal. Chem. 12 (1998) 681–693.
[6] A. Pawelec, B. Strojek, G. Weisbrod, S. Podsiadlo, Ceram. Int. 28 (2002) 495–501.
[7] T. Jaschke, M. Jansen, J. Mater. Chem. 16 (2006) 2792–2799.
[8] F. Cheng, S.M. Kelly, F. Lefebvre, S. Clark, R. Supplit, J. Bradley, J. Mater. Chem. 15 (7) (2005) 772–777.
[9] M.A. Schiavon, G.D. Soraru, I.V. Yoshida, J. Non-Crystal. Solids 348 (2004) 156–161.
[10] E. Kroke, M. Schwarz, Coord. Chem. Rev. 248 (2004) 493–532.
[11] Y.C. Zhao, D.L. Yu, H.W. Zhou, Y.J. Tian, O. Yanagisawa, J. Mater. Sci. 40 (2005) 2645–2647.
[12] I. Umezu, T. Yamaguchi, K. Kohno, M. Inada, A. Sugimura, Appl. Surf. Sci. 197–198 (2002) 376–378.
[13] Q. Guo, Q. Yang, L. Zhu, C. Yi, S. Zhang, Y. Xie, Solid State Commun. 132 (2004) 369–374.
[14] H. Montiguad, B. Tanguy, G. Demazeau, I. Alves, M. Birot, J. Dunogues, Diamond Relat. Mater. 8 (1999) 107–1710.
[15] B. Jurgens, E. Irran, J. Senker, P. Kroll, H. Muller, W. Schnick, J. Am. Chem. Soc. 125 (2003) 10288–10300.
[16] X. Wu, Y. Tao, Y. Lu, L. Dong, Z. Hu, Diamond Relat. Mater. 8 (2006) 164–170.
[17] C. Balazsi, Z. Konya, F. Weber, L. Biro, P. Arato, Mater. Sci. Eng. C 23 (2003) 1133–1137.
[18] D.M. Teter, R.J. Hemley, Science 271 (1996) 53.
[19] M. Leidl, C. Schwarzinger, J. Anal. Appl. Pyrol. 74 (2005) 200–203.
[20] C.W. Chen, C.C. Huang, Y.Y. Lin, L.C. Chen, K.H. Chen, Diamond Relat. Mater. 14 (2005) 1126–1130.